

# Toughness enhancement in polymer blends due to the *in-situ* formation by chaotic mixing of fine-scale extended structures

Y. H. LIU, D. A. ZUMBRUNNEN\*

Center for Advanced Engineering Fibers and Films, Department of Mechanical Engineering, Clemson University, Clemson, SC 29634-0921, USA  
E-mail: zdavid@ces.clemson.edu

Experimental results are presented to demonstrate that significant improvements to the impact properties of a polystyrene (PS) matrix can be achieved by the addition of only 9% by volume of low density polyethylene (LDPE). Polymer blends of LDPE and PS were combined in the molten state within a cylindrical cavity where a quiescent, three-dimensional chaotic mixing process was performed. Whereas a minor phase normally adopts the form of highly distributed droplets in conventional processing techniques, minor phase bodies were stretched and folded recursively to yield fine-scale extended and interconnected structures. The structures were largely preserved upon solidification. Impact tests were carried out on specimens which were machined from the solidified blend. Fracture surfaces of the impact test specimens were examined by scanning electron microscopy. Blends achieved a maximum impact toughness 69% higher than that of PS. Results demonstrate potential improvements in properties that may be obtained if favorable and unique microstructures are formed directly in the melt during processing. © 1999 Kluwer Academic Publishers

## 1. Introduction

Polymer blends have drawn much attention for the last two decades, as blending generally provides a more economic way to achieve requisite properties than does synthesizing new polymer resins. When polymers are combined in the melt state to enhance a physical property, forceful mixing is most often used. For example, extruders and batch mixers are employed to make polymer blends from component resins in order to manufacture a wide range of plastic products. Because the mixing occurs forcefully, structures defined by elongated fluidic interfaces are broken down so that a molten minor phase eventually takes the form of distributed droplets. Polyethylene (PE) and polystyrene (PS) blends are among the most studied polymer blends because they are deemed to be typical immiscible blends, and because both PE and PS are common thermoplastics. In addition, polymer recycling is an area of growing interest. Both PE and PS are major constituents of plastic waste, which respectively consist of about 60 and 15% by weight of all recycled plastics [1]. Creating a PE/PS blend with attractive mechanical properties is therefore important for reducing plastics wastes. Results of this research demonstrate in particular the potential improvements in impact properties that may be obtained if new and desirable microstructures can be developed directly in the melt and captured by solidification.

As an immiscible blend, a PE/PS blend usually does not have attractive mechanical properties owing to poor stress transfer between component phases which lack interfacial adhesion. Ramos and Collar [2] studied low density polyethylene (LDPE)/PS blends with various compositions without adding any compatibilisers. It was found that both tensile and yield strengths of 15 wt % LDPE/PS blend were less than one half of those of pure PS. Both tensile and yield strengths were also noticeably lower than those of pure LDPE. The impact toughness of the blend, however, was only about 25% higher than that of pure PS, despite the fact that the impact toughness of LDPE was eight times higher than that of PS. Schwarz, *et al.* [3] studied the mechanical properties of high density polyethylene (HDPE)/PS blends. It was found that adding up to 75 wt % of HDPE with or without a compatibiliser failed to improve the impact property of PS, although HDPE is about three times tougher than PS.

As pointed out by Teh and Rudin [4], mechanical properties of PE/PS blends such as tensile and yield strengths, modulus, elongation at break, and impact toughness were rarely better than those of the pure PS counterparts. In their study, a 10 wt % PE/PS blend was made using a twin-screw extruder, then impact specimens of the blend were prepared with either compression molding or injection molding. Minor phase bodies formed highly distributed spherical droplets after

\* Author to whom all correspondence should be addressed.

extrusion and then were elongated to some extent during molding. Impact properties changed with the extrusion conditions. The impact toughness decreased slightly with increasing screw speed since more refined droplets were formed that became less elongated upon injection molding. The impact toughness was also lower at low mass flow rates where extended residence times allowed further break-up of the elongated domains and also resulted in more refined and less elongated droplets. It is interesting to note that blend samples had poorer impact toughness than a pure PS sample except one prepared directly by injection molding without passing through the twin-screw extruder. For this blend, the unnotched sample had an impact toughness 37% higher than that of PS; its notched sample, however, was inferior to the PS counterpart. The relatively good toughness of unnotched specimens was attributed to a fibrillar structure in the skin of the specimen. The inferior core structure with coarse phase domains was exposed in the notched specimens; thereby a poor impact property was exhibited.

All these results reveal that highly dispersed droplets resulting from extensive mixing typical of a twin-screw extruder are not an ideal morphology for achieving good mechanical properties. An optimal structure might well be one with extended lamellar or fibrillar morphologies such that greater impact forces can be borne by the tough LDPE phase. It is particularly important for immiscible blends to develop favorable microstructures in order to acquire attractive mechanical properties. Microstructures which contain minor phase bodies of large aspect ratios will compensate for poor interfacial adhesion and thus provide improved stress transfer. Unfortunately, favorable extended microstructures usually cannot be obtained by conventional melt processing methods like extrusion. Minor phase bodies are usually broken down to highly distributed droplets at the beginning of processing. Lindt and Ghosh [5], for example, studied both a miscible blend and an immiscible blend in a single screw extruder and saw in the melting zone that the striation thickness decreased abruptly from about  $200\ \mu\text{m}$  to  $5\ \mu\text{m}$  for both blends. Plochocki, *et al.* [6] studied the LDPE/PS blend with and without a compatibilizer in both single-screw and twin-screw extruders. They also found that the morphology development was essentially complete in the melting zone. Scott and Macosko [7] and Sundararaj *et al.* [8] proposed an explanation about the dramatic changes in morphology which occurred in the softening and melting stages. Polymer pellets melted on the hot surface and were dragged into thin sheets with thicknesses on the order of microns. Holes then formed in the thin sheets and grew into a lace-like structure. This structure soon fragmented into spherical droplets.

Although fibers can be formed in extensional flows which exist at the converging entrance of a die or in an injection mold, the minor phase concentration must be high [9]. At low concentrations, minor phase droplets formed in an extruder do not undergo sufficient coalescence before arriving at the entrance of the die. Such small minor phase droplets can not be stretched effec-

tively to form fibrils. Numerical simulations and experiments have shown that effective stretching occurs at high capillary numbers for which interfacial tension is small in comparison to viscous forces [10, 11]. Since the capillary number is proportional to initial droplet diameter, small droplets which do not undergo agglomeration may largely define the ultimate microstructure upon solidification of the melt.

In this study, chaotic mixing was used as an especially effective means to gently combine polymeric melts. Under global chaotic mixing conditions, individual fluid particles move along unique paths and minor phase bodies are recursively stretched and folded as a consequence. A computer simulation of the transition from regular to chaotic motion of fluid particles in a melt is shown in Fig. 1 in a cylindrical cavity specifically designed for producing materials with very fine-scale internal structures [12]. These panels are known as first-return maps since the successive positions of a single particle are shown at the conclusion of successive mixing periods. Regular motion is indicated when the particle motion defines a loop; whereas chaotic motion is indicated when the particles move to new positions. Chaotic motion can be instilled by simple periodic motions of the cavity walls described by the perturbation strength  $\mu$  which will be subsequently defined. Fig. 1 shows that as  $\mu$  gradually increases, the motion of particles changed from periodic to chaotic. It is clear that as chaos prevails, particles no longer follow regular paths. Instead, the particle motion fills the entire cavity. Because neighboring particles constituting minor phase bodies also move along their own unique paths, adjacent particles separate rapidly from each other resulting in high stretching rates and folding of minor phase bodies. The resulting reduction in length scale and emergence of a distributed minor phase structure due to repetitive stretching and folding is also depicted in Fig. 1. Physical mechanisms for the development of fine-scale lamellar and fibrillar structures in polymer melts mixed within this cylindrical cavity have been reported previously [13, 14]. The formation in melts of fibers from sheets and the break up of fibers to droplets have been simulated computationally and general characteristics agreed with those of experiments [15, 16].

The efficiency of chaotic mixing makes possible the creation of highly stretched structures in response to gentle and simple motions of bounding surfaces. Minor phase pellets were stretched rapidly into thin sheets at the early stage of mixing. Fibers were subsequently formed within folds and edges of these sheets. Since fibers eventually subdivided into droplets due to capillary instabilities, droplets were commonly intermingled with fibers at relative abundances dependent on the processing and solidification times. Microstructures were produced having different relative abundances of fibers, sheets, and droplets of different sizes. Impact properties for these different microstructures were individually measured and characterized to disclose potential enhancements that might be obtained if similar microstructures can be produced in industrial processes.

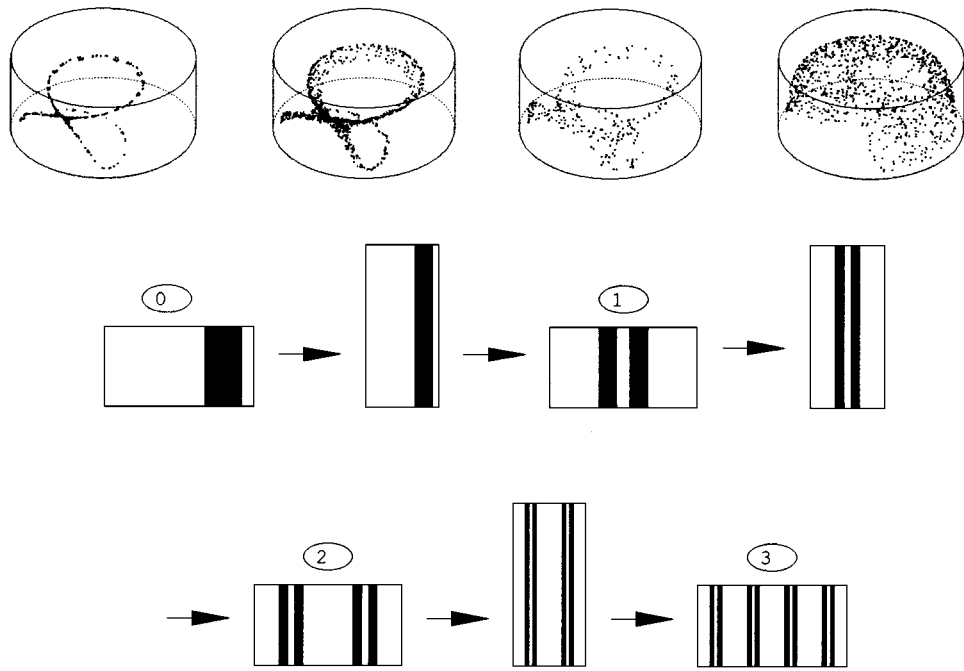


Figure 1 Computer simulated transition to chaotic motion in fluid particles contained in a cylindrical cavity used to generate fine-scale structures in melts [12].

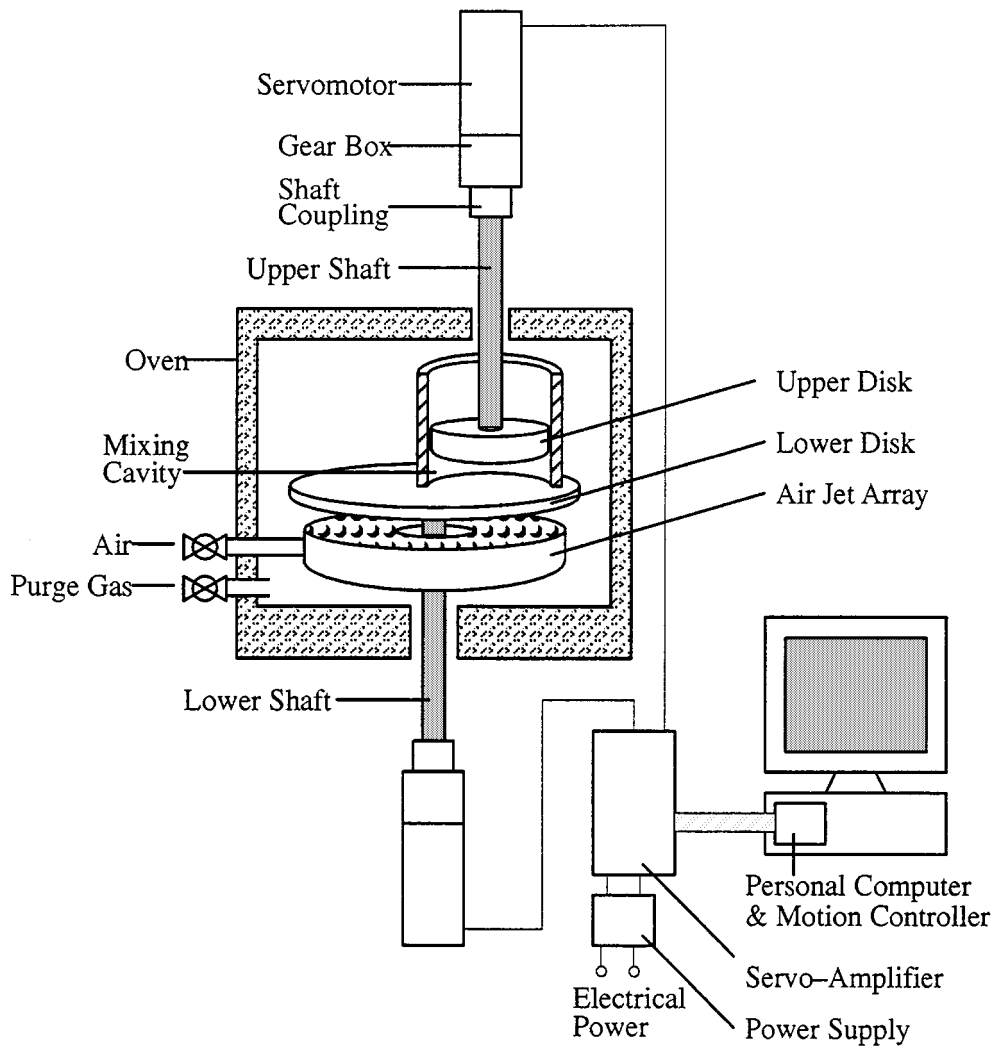


Figure 2 Schematic of mixing apparatus.

## 2. Experimental methods and materials

A simple, effective, and easily operated apparatus intended for polymer melt mixing is shown schematically in Fig. 2. Three-dimensional chaotic advection was induced in the melt which was confined within a cylindrical cavity. The cavity was formed between rotatable upper and lower circular disks and a stationary lateral cylindrical surface. The elevation of the suspended concentric upper disk could be adjusted to vary the height  $H$  of the mixing cavity. Since the inner diameter  $D$  was fixed at 48 mm, the aspect ratio  $A$  of the mixing cavity, which was defined as  $H/D$ , varied with  $H$ . The offset distance  $E$  of the lower shaft from the cylindrical center of the cavity could also be adjusted to change the eccentricity  $e$ , which was defined as  $2E/D$ . Each disk rotated independently at an angular speed  $\omega$ . The rotational displacement in terms of the fraction of a complete rotation within each mixing period for either the upper or lower disk defined the perturbation strength  $\mu$ . For all tests of this study, these parameters were kept constant, with  $A = 0.3$ ,  $e = 1.6$ ,  $\mu = 1.2$ , and  $\omega = 1$  rpm. Details about the apparatus and the verification of chaotic advection were subjects of a prior study [12].

Mixing protocol deals with the sequence of disk rotations and is very important to the mixing efficiency. Two mixing protocols were adopted in this study. One was a periodic sequence, starting with the rotation of the lower disk and following with the rotation of the upper disk in the opposite direction. One pair of rotations of the lower and upper disks fulfilled one mixing period. Rotations were continued for the prescribed number  $N$  of periods with the upper disk rotating last. The periodic sequence can be represented as LU LU . . . LU, where L and U denote the rotation of the lower and upper disks, respectively. Another mixing protocol used in the study was a more complicated symmetry-breaking sequence [17, 18], where a sequence segment is always attached by its complement segment of the same length. For instance, a symmetry-breaking sequence for  $N = 10$  can be represented as LU UL UL LU UL LU LU UL UL LU. Symmetry-breaking protocols are more effective than the simple periodic protocol in promoting uniform mixing conditions in a symmetric cavity [19]. This has been experimentally verified for the mixing cavity of Fig. 2 by combining pigmented and unpigmented LDPE. A more rapid decrease in the striation thickness of the pigmented minor phase occurred when using a symmetry-breaking protocol instead of a periodic protocol.

In this study, 9 vol % LDPE (Tenite 18DOA, Eastman Chemical Co., Kingsport, TN, USA) was added into a PS matrix (GPPS 555, Novacor Chemical Inc., Leominster, MA, USA) to improve the impact property. The viscosity ratio  $\lambda$ , which was defined as the viscosity of minor phase divided by the viscosity of the major phase, was about 0.2 at the processing temperature of 180 °C. In order to reduce the interfacial tension, 1 vol % compatibiliser was also added to the blend. A block copolymer of styrene-ethylene/butylene-styrene (SEBS, Kraton G1652, Shell Chemical Co., Houston, TX, USA) was selected as the compatibiliser because of its reported effectiveness over other copolymer compatibilisers [4, 20–22]. Pellets of LDPE were frozen with

liquid nitrogen and ground to reduce the pellet size so that finer microstructures could be obtained at less mixing periods. Ground pellets of 1–2 mm diameter were selected by sifting. The selected LDPE pellets were then mixed at room temperature with SEBS powders by mechanical stirring in a beaker at a volume ratio of 9 : 1. This mixture was combined with the PS pellets and mechanically mixed at a volume ratio of 1 : 9. The well distributed pellets and powders were then melted in a 37 mm diameter cylinder and allowed to solidify. This diameter matched the diameter of the mixing cavity in the apparatus of Fig. 2. The void-free lower portion of the cylindrical ingot was cut to meet the prescribed aspect ratio for the processing sample. The disk-shaped ingot was then pressed into the cavity and heated. Mixing was started after one hour to ensure that a uniform melt temperature was reached. Two pure PS samples were also produced for comparison. To ensure that these pure PS samples experienced the same thermal history as other samples of LDPE/PS blends, the PS samples were also melted, kept for one hour, to reach a uniform temperature distribution in the melt, mixed for 20 periods in the mixing cavity of Fig. 2, and solidified.

The capture upon solidification of the melt structures which emerged during mixing was a key to successful property enhancement. Melt structures were largely preserved during the course of mixing because agitations were gently applied. The slow process also allowed enough time for compatibiliser to diffuse to the phase interfaces. The existence of compatibiliser at interfaces reduced the interfacial tension and thus helped to stabilize the microstructure. However, extended structures of minor phase bodies tended to fragment into droplets when the induced cavity flows subsided [10, 23]. It was therefore important to ensure that the time scale for fragmentation was longer than the cooling period. A companion study [15] revealed that the fragmentation time scale could be extended by increasing the melt viscosity. Thus, a low processing temperature of 180 °C was chosen such that the melt viscosity was high and the fragmentation time scale was long. The low processing temperature also reduced the chance of melt decomposition since mixing times as long as about 1 hour were used.

Each solidified sample was sliced into two identical thin disks which were further cut vertically to the disk plane along the symmetric line that contained the rotational axes of the shafts in Fig. 2. Thus, four rectangular specimens of  $19.1 \times 12.7 \times 3.18$  mm<sup>3</sup> were obtained from one original sample, with specimens #1, #2 from the lower portion of the disk and #3, #4 from the upper portion, as shown in Fig. 3. The impact strengths of these rectangular specimens were tested in accordance with the ASTM D 4508-93 standard. Tests were carried out on a GRC8200 DYNATUP drop weight impactor, and the experimental data were collected and processed by a personal computer running a companion software called DYN830. Both the impactor and the software were developed by General Research Corporation (Santa Barbara, California, USA).

Prior to a test, a cross head with a tup (i.e., an impact hammer) was raised to an identical drop height. The specimen was clamped by a steel specimen holder

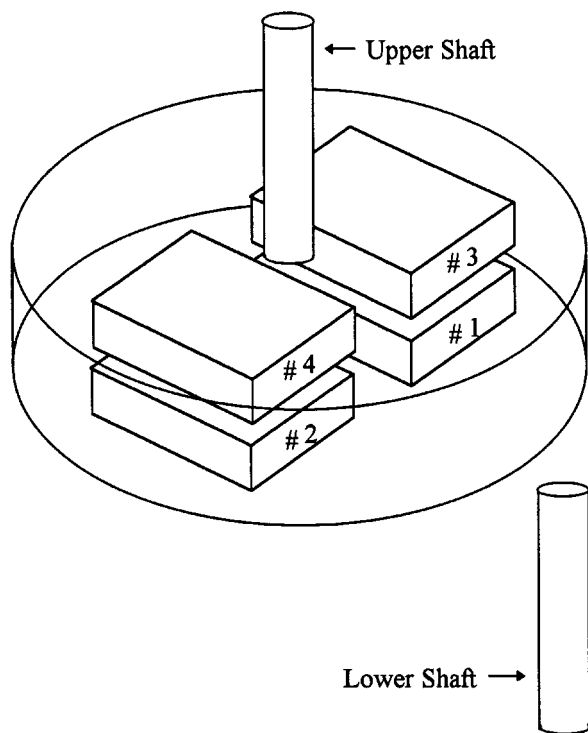


Figure 3 Relative positions of impact specimens cut from a disk-shaped sample taken from the mixing cavity of Fig. 2.

which was in turn clamped to a fixture on the base of the impactor. The cross head was released and underwent a free fall as the friction from the guide cylinders was negligible. Just before the tup hit the specimen, a sensor recorded the speed of the cross head and triggered the data requisition system. The impact force  $F$  (load) acting on the tup was recorded over the next 20 ms and more than 2000 data points were collected. The instantaneous acceleration of the tup was computed from the recorded load  $F$  and the mass of the cross head assembly. The instantaneous velocity of the tup was subsequently calculated from the acceleration and the initial velocity which had been recorded by the sensor. Assuming a close contact between the tup and the specimen was maintained from the moment of impact to the failure point, the deflection of the specimen was obtained by integrating the tup velocity over the time  $t$ . The absorbed energy  $W$  was computed from the loss of the kinetic and potential energy of the cross head assembly after impact. Full fractograms of tup velocity, specimen deflection, load  $F$ , and absorbed energy  $W$  were obtained. These fractograms promoted more complete understanding of the material behavior under impact and ensuing failure, and of the relationship between the material properties and microstructures.

As reported here, the impact toughness  $w$  is a measurement of absorbed energy per unit area of the fracture surface. Besides  $w$ , two other properties were documented in order to reveal the impact behavior more completely. The first property concerned the peak stress which the specimen withstood under impact, and was denoted by  $f$  which equaled the maximum load  $F$  divided by the cross-sectional area of the specimen. The second documented property was the time period  $t_f$  from impact to failure. The ductility of the materials,

which can be considered as the strain at break, was well reflected by  $t_f$  since the deflection was almost linearly proportional to time. To promote uniformity in measurement conditions, the drop height was fixed at about 6 cm, such that the impact velocity was 1.06 m/s. The total weight of the cross head and tup assembly was 3.608 kg, and the capacity of the assembly was 2.07 J for this given drop height.

Fracture surfaces were examined with a JOEL JSM IC484 scanning electron microscope (SEM). Specimens were sputter coated with a thin layer of gold prior to observation. All micrographs are oriented such that the impact surface is the upper portion and the direction of crack propagation was from the top to the bottom of the micrographs. Minor phase structures were also liberated by dissolution of specimens in xylene. The extracted minor phase was deposited on an aluminum plate and examined under SEM.

### 3. Results and discussion

The behavior of the pure PS and LDPE/PS blends to the impact tests will be presented first as functions of the number of processing periods  $N$ , since the microstructural development during chaotic mixing of the major and minor phases depended on the processing time. Micrographs will be subsequently presented to relate mechanical properties to specific microstructures. Pure PS specimens were tested to provide baseline results of impact toughness  $w$ , peak impact stress  $f$ , and failure time  $t_f$ . All other test results of blends will be presented relative to this baseline. The fractograms of eight specimens were identical in shape and differed by small amounts in magnitude. One of the fractograms is shown in Fig. 4. The impact load  $F$  was initially zero as no force was measured by the sensor before impact. At  $t = 0$ , the tup impacted the specimen, and  $F$  increased linearly with  $t$ . The load  $F$  reached a peak of about 200 N in 0.63 ms, and then abruptly plunged to zero due to brittle fracture. However, the fracture point was not defined as the moment when  $F$  dropped to 0, because the kinetic energy of the fractured specimen (i.e., the toss energy) would lead to an over-estimation of the impact toughness. The fracture point was defined

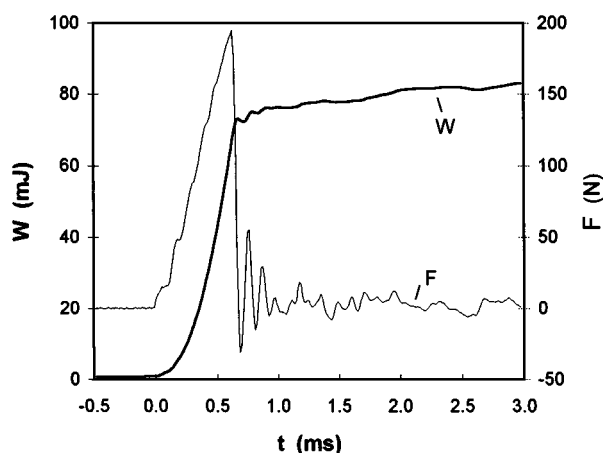


Figure 4 Impact fractogram for load and absorbed energy of a pure polystyrene specimen.

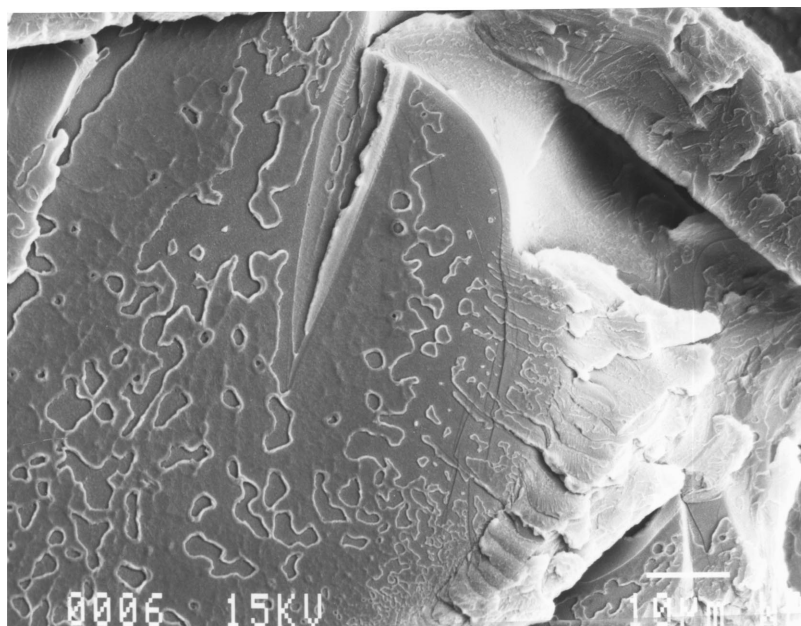


Figure 5 Electron micrograph of a characteristic fracture surface of a pure polystyrene specimen.

TABLE I Impact testing results of pure PS specimens

	Impact toughness (kJ/m <sup>2</sup> )	Impact strength (MPa)	Time to failure (ms)
Mean	1.74	4.67	0.65
Standard deviation	0.31	0.46	0.04

instead as the moment when  $F$  declined to 30 percent of the maximum load, which was suggested as the default choice in DYN830 data processing software. The load signals recorded after the fracture (i.e.  $t > 0.66$  ms) reflected the aftershock vibrations of the tup. The mean values and standard deviations of the  $w$ ,  $f$  and  $t_f$  of eight pure PS specimens are presented in Table I. The deviations were attributed to the intrinsic unsteady characteristics of the impact test and factors such as slight differences existing in specimen geometry and dimensions. The fracture surface for a pure PS specimen is shown in Fig. 5. Very little deformation is exhibited on the fracture surface, indicating a brittle fracture which has been illustrated by the fractogram shown in Fig. 4.

The impact toughness  $w_B$  of the LDPE/PS blend is presented relative to the impact toughness  $w_{PS}$  of the pure PS specimens in Fig. 6. The data point at  $N = 0$  is the average result for the blend without mixing in the apparatus of Fig. 2. The minor phase domains in these specimens remained as the initial undeformed pellets of 1–2 mm diameter which were mechanically mixed as described previously. Since stress could not be transferred efficiently across the weak LDPE/PS interface, the coarse LDPE domains acted essentially as holes and thus considerably weakened the PS matrix. Experimental results showed that impact toughness decreased to about one-half of that for pure PS specimens, i.e.,  $w_B/w_{PS} = 0.5$  for  $N = 0$  in Fig. 6.

After processing by chaotic mixing, the impact properties of the LDPE/PS blends improved significantly

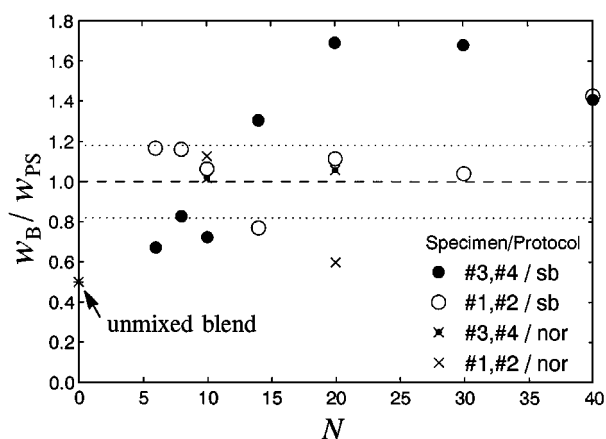


Figure 6 Variation of impact toughness of 9 vol % LDPE/PS blends after completion of different numbers of mixing periods ( $N = 0, 6, 8, 10, 15, 20, 30,$  and  $40$ ).

due to the formation of extended interfacial structures. After only 6 periods of mixing,  $w_B/w_{PS}$  increased from 0.50 to 0.92. Although  $w_B$  reached the same level as  $w_{PS}$ , the standard deviation of the impact toughness of eight specimens was twice as much, indicating a lack of structural uniformity in the blend. The major contribution to the large standard deviation came from the difference in toughness existing between the upper specimens 3 and 4 and lower specimens 1 and 2 (Fig. 2). Differences for the two upper specimens or for the two lower specimens was not as significant. The average  $w_B/w_{PS}$  of the two upper specimens is shown as a solid circle in Fig. 6, while results for the two lower specimens was shown as an open circle. For  $N = 6$ ,  $w_B/w_{PS}$  equaled 0.67 for the upper specimens and 1.17 for the lower specimens. As the number of mixing periods increased,  $w_B/w_{PS}$  of the lower specimens showed a slight initial decrease, and a gradual increase after  $N = 14$ . In contrast,  $w_B/w_{PS}$  of the upper specimens increased steadily with the number of mixing periods until a maximum value of 1.69 for  $N = 20$  was obtained, after

which a decline occurred for  $N > 30$ . For  $N = 40$ , the toughness of both the upper and lower specimens were nearly identical. Toughness was enhanced by about 40% relative to pure PS. Small differences in the toughness occurred since uniformity in the microstructures arose after sufficient mixing had been performed. It is worth noting that despite the unsuccessful efforts of other research groups in toughening PS with about 10 wt % PE using conventional melt processing techniques [2–4], specimens 3 and 4 prepared with chaotic mixing achieved a toughening enhancement as high as 69% with the addition of only 9 vol % (i.e., about 8 wt %) of PE.

The peak impact stress  $f$ , which indicated the maximum load a specimen withstood upon impact, was another property of interest. It is normally expected that the addition of a soft LDPE phase should yield a blend with a peak impact stress less than that for pure PS. However, since PS fractures under impact at stresses much lower than its static strength, an addition of tough LDPE potentially could enhance  $f$ . The dependence of the ratio  $f_B/f_{PS}$  on the number of mixing periods is shown in Fig. 7. The upper specimens displayed a trend for  $f_B/f_{PS}$  similar to the one for  $w_B/w_{PS}$ . The ratio  $f_B/f_{PS}$  increased steadily with the number of mixing periods until it reached a peak of 1.24 for  $N = 20$  then declined slightly afterwards. Lower specimens, on the other hand, had generally increasing  $f_B/f_{PS}$  with the number of mixing periods  $N$ . Again, after prolonged mixing for 40 periods, the lower specimens had an average  $f_B/f_{PS}$  of 1.07, which was very close to the value of 1.10 for the upper specimens.

In Fig. 7, the lower specimens of Fig. 3 generally had lower peak impact stresses than did the upper specimens. However, as shown in Fig. 6, the lower specimens had higher toughnesses when the number of mixing periods was small. Since the absorbed energy  $W$  is the integration of the load  $F$  over the displacement, the lower specimens for  $N < 10$  deformed more during impact tests and consequently had longer elapsed times  $t_f$  to failure, as verified in Fig. 8. The longer  $t_f$  for the lower specimens was due to lamellar structures which will be discussed later in association with impact fractograms and electron micrographs. For small

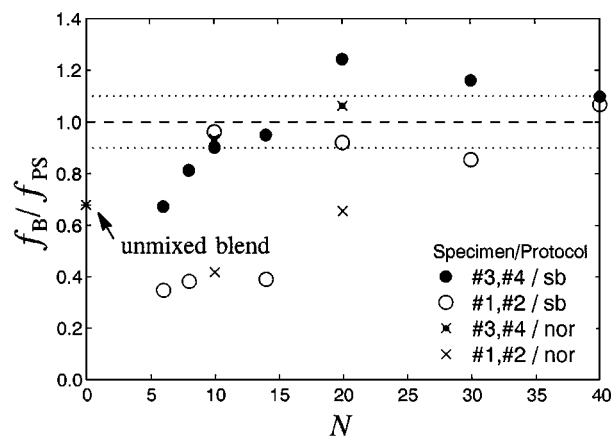


Figure 7 Variation of peak impact stress of 9 vol% LDPE/PS blends after completion of different numbers of mixing periods ( $N = 0, 6, 8, 10, 15, 20, 30,$  and  $40$ ).

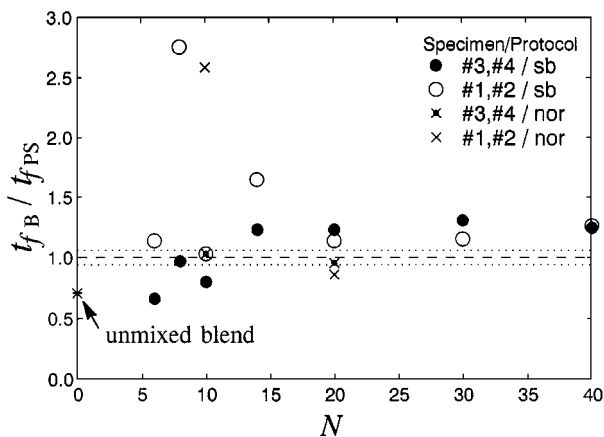


Figure 8 Variation of failure time of 9 vol% LDPE/PS blends after completion of different numbers of mixing periods ( $N = 0, 6, 8, 10, 15, 20, 30,$  and  $40$ ).

$N$ ,  $t_f$  was always longer for lower specimens than for upper specimens. As  $N$  increased, the ratio  $t_{fB}/t_{fPS}$  in Fig. 8 for the lower and upper specimens approached the same value. After  $N \geq 20$ , the difference in  $t_f$  between the lower and upper specimens was small. For  $N = 40$ , the average value of  $t_{fB}/t_{fPS}$  was 1.25 for the upper specimens and 1.26 for the lower ones. The fact that LDPE/PS blends had longer elapsed times to failure than pure PS specimens indicated that the blends were more ductile.

A more comprehensive understanding of the impact behaviour and its relationships with the microstructure can be gained by closely studying the fractograms and micrographs of fractured surfaces. Specimens mixed for small numbers of periods were of particular interest because the mixing was incomplete and interfacial structures developed most rapidly. Fractograms of the upper and lower specimens of the LDPE/PS blend for  $N = 6$  are shown in Fig. 9. The load fractogram of the upper specimen (i.e.,  $F$  versus  $t$  in Fig. 9a) appeared similar to that of the pure PS specimen (Fig. 4), indicating that the specimen had a uniform structure. On the other hand, the load fractogram of the bottom specimen (Fig. 9b) had a succession of small peaks after the major load peak, which was a signature of intermittent crack propagation. Scanning electron micrographs (Fig. 10a) showed that the upper specimen had a relatively uniform fibrillar structure, whereas the lower specimen had a lamellar structure (Fig. 10b). In the lamellar structure, PS layers were separated by thin LDPE layers. These tough LDPE layers stopped the crack from propagating from one PS layer directly to the next PS layer. The fracture of each PS layer was detected as an individual peak on the fractogram of Fig. 9b. The total fracture time of the specimen was substantially increased since the fracture was interrupted repeatedly by tough LDPE layers. The micrograph also showed that LDPE layers underwent extensive deformation upon rupture. The energy needed to rupture these LDPE layers contributed to the high toughness of the specimen.

For larger numbers of mixing periods, the morphology of the minor phase changed from sheets to fibrils and eventually to droplets. A close inspection of the micrograph in Fig. 10b revealed that the microstructure of

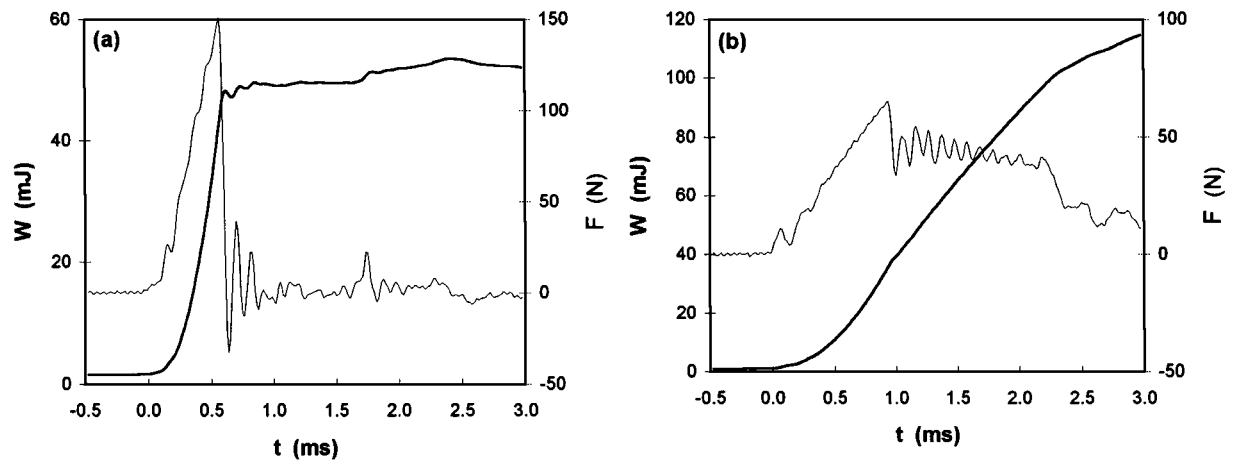
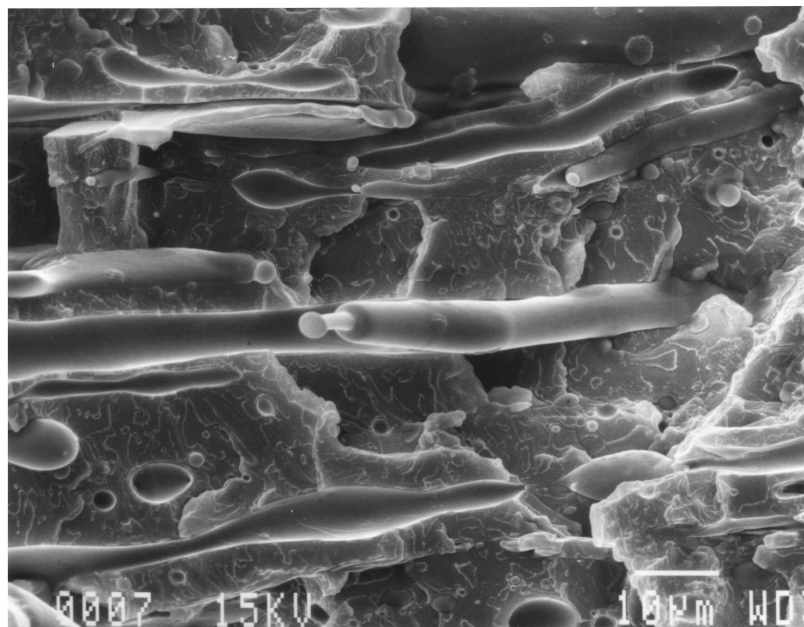
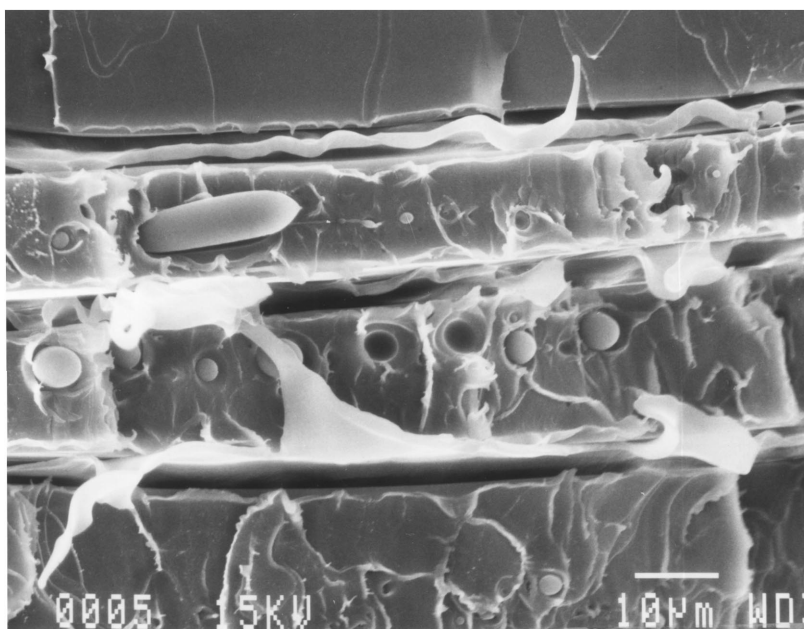


Figure 9 Impact fractograms of 9 vol% LDPE/PS blend mixed with the symmetry breaking protocol ( $N = 6$ ) (a) upper specimen #3, (b) lower specimen #2.



(a)



(b)

Figure 10 Electron micrographs of 9 vol% LDPE/PS blend mixed with the symmetry breaking protocol ( $N = 6$ ) (a) fibrous morphology in upper specimen #3, (b) lamellar morphology in lower specimen #2.

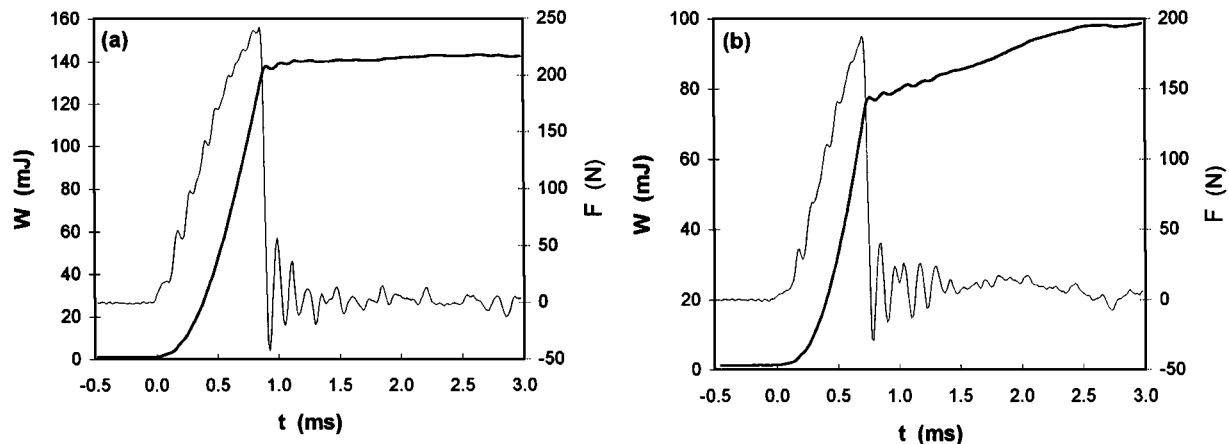


Figure 11 Impact fractograms of 9 vol% LDPE/PS blend mixed with the symmetry breaking protocol ( $N = 20$ ) (a) upper specimen #4, (b) lower specimen #2.

the bottom specimen for  $N = 6$  was not simply lamellar. Fibrils and droplets of LDPE with diameters ranging from 1 to 10  $\mu\text{m}$  were evident inside the PS layers. Companion studies [14–16] have shown that the morphology of the minor phase changed continuously as mixing proceeded. At the early stages of mixing, the dimensions of minor phase bodies were large and the viscous force was dominant over interfacial tension. As a consequence, minor phase bodies were rapidly stretched into sheets. With the decrease in dimensions of the minor phase bodies, the interfacial tension became more significant. Fibrils started to be formed within the folds and edges of sheets. As sheets broke down into fibrils, fibrils also fragmented into droplets due to capillary instabilities. Therefore, the morphology generally consisted of sheets, fibrils, and droplets, with the proportion of sheets decreasing and the proportion of the droplets increasing with processing time. For very long mixing times, the lamellar structure disappeared and dispersed droplets characterized the microstructure. Such dispersed droplet microstructures are typical in blends produced by conventional mixing processes.

The change in the morphology from lamellar to droplet was reflected in the fractograms of Fig. 11 for LDPE/PS blends mixed for 20 periods. The shape of the fractogram of the upper specimen (Fig. 11a) was similar to that of the upper specimen for  $N = 6$  (Fig. 9a). A higher peak value for  $W$  indicated property improvement with processing time. However, the successive peaks of high magnitude in the lower specimen for  $t > 1$  ms in Fig. 9b which were associated with the lamellar structures did not appear for the lower specimen in Fig. 11b. Fracture instead occurred abruptly after the maximum stress was reached, indicating the absence of continuous lamellar structures due to the longer processing time.

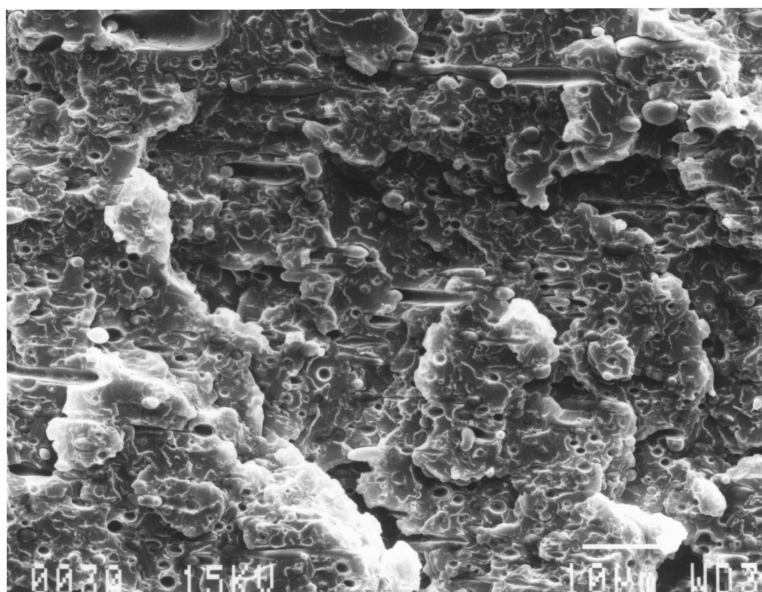
Despite the similar shapes of the fractograms for the upper and lower specimens in Fig. 11 with  $N = 20$ , both toughness and peak impact stress of the lower specimens were noticeably lower than those of the upper specimens. These differences can be explained by the differences in the microstructures. Fig. 12 reveals that the upper specimen had a much more refined structure

than did the lower specimen. Fibrils of a few microns in diameter were also abundant on the fracture surface of the upper specimen. Some fibrils perpendicular to the fracture surface are shown in cross-section and should not be mistaken as droplets. Long and fairly uniform fibrils were clearly exposed where the matrix had been removed by a solvent. Since the fine-scale fibers had high aspect ratios and large interfacial areas, stress was efficiently transferred between phases. Thus, the impact property of the blend was significantly enhanced.

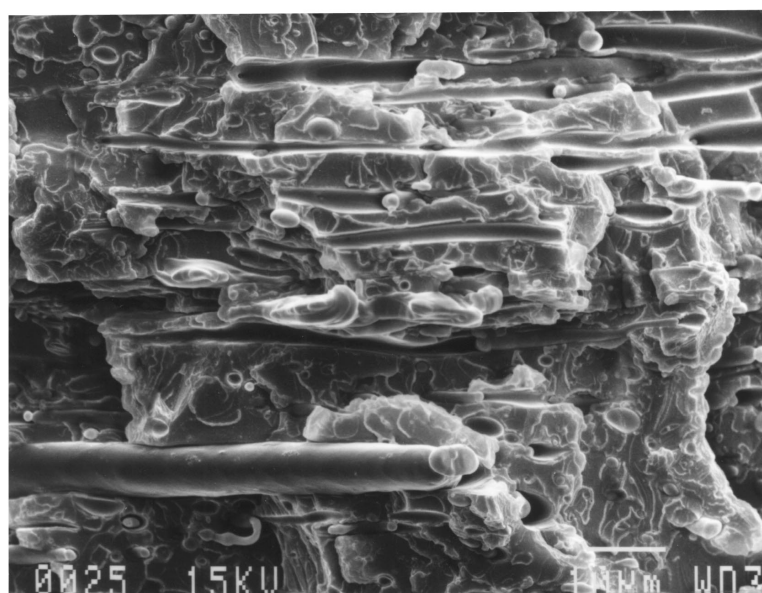
Blends with higher LDPE concentrations were also tested in order to investigate the morphology and property dependency on composition. For 27 vol% LDPE/PS blends mixed for 20 periods, the minor phase LDPE and the major phase PS were co-continuous. Fibrils of PS were abundant on the fracture surface shown in Fig. 13. Fibrils and sheets of the minor phase LDPE were also evident on the fracture surface. Thus, it is interesting to note that both the major and minor phases assumed a fiber form in the melt. This novel microstructure arose since sheets were first formed in both phases which subdivided due to interfacial instabilities leading to the formation of fibers [15, 16]. With 27 vol% LDPE, the blend was about twice as tough as pure PS, with  $w_B/w_{PS} = 1.99$  for the lower specimens and 2.19 for the upper specimens. However, due to the relatively high LDPE loading, the blend had a lower peak impact stress, with  $f_B/f_{PS} = 0.44$  for the lower specimens and 0.52 for the upper specimens. The blend was also much more ductile than the pure PS, with  $t_{fB}/t_{fPS} = 4.03$  for the lower specimens and 3.63 for the upper specimens. Inverse blends consisting of 9 vol% of PS in the LDPE matrix were also studied. Fibrils of PS were found in the continuous LDPE phase. The blends were soft and ductile and did not undergo complete fracture under impact. Notably, similar microstructures were produced irrespective of which polymer was the major phase.

#### 4. Conclusions

The toughness characteristics of unique microstructures formed at low minor phase concentrations were systematically investigated. A processing method was used which may be particularly attractive where



(a)



(b)

Figure 12 Electron micrographs of 9 vol % LDPE/PS blend mixed with the symmetry breaking protocol ( $N = 20$ ) (a) fine fibrillar structure of upper specimen #4, (b) fibrillar structure of lower specimen #2.

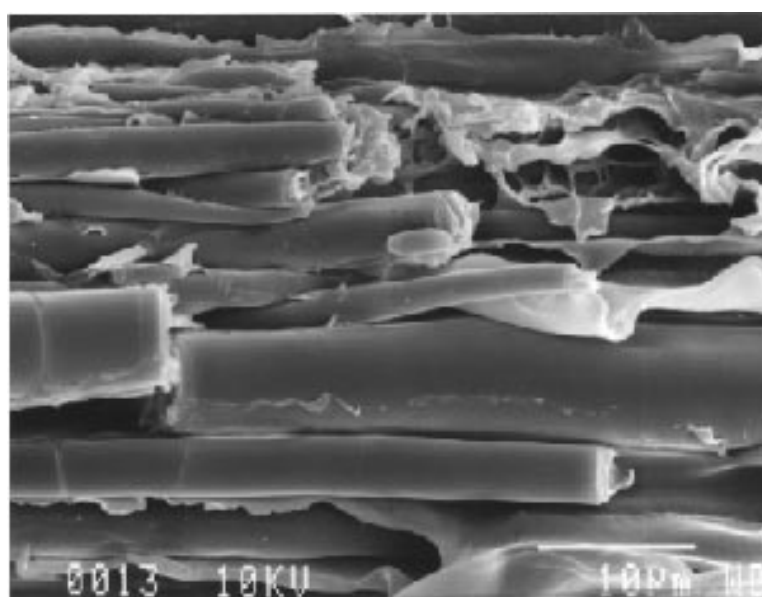


Figure 13 Electron micrographs of 27 vol % LDPE/PS blend mixed with the symmetry breaking protocol ( $N = 20$ ).

polymers are incompatible and interfacial characteristics are poor. Unlike conventional melt processing, mixing occurred gently so that extended fine-scale structures defined by fluidic interfaces formed in the melt and were captured by solidification. Chaotic mixing was used as an especially effective means to generate fine-scale structures in melts. The relationship between the microstructures and impact properties of polymer blends consisting of a 9 vol % LDPE minor phase, 1 vol % SEBS compatibiliser, and a PS matrix was specifically considered. Experimental results demonstrated that the blend microstructure changed from lamellar to fibrillar, and eventually fragmented into spherical droplets if mixing was continued. Various impact properties were obtained by stopping the mixing after different numbers of mixing periods ( $N$ ). For  $N < 20$ , lamellar structures were produced which were characterized by high impact toughnesses and long fracture times. When mixing was performed for considerably longer periods ( $20 < N < 30$ ), fibrillar structures arose which provided greater improvements in impact properties. For specimens with the finest extended microstructures, toughness was 69% higher, peak impact stress was 24% higher, and failure time was 23% longer than specimens of pure PS. For very long mixing times, the extended structures subdivided and a dispersed droplet morphology in the minor phase appeared. Such microstructures are characteristic of conventional melt processing techniques and were associated with little improvement or decreases in toughness.

### Acknowledgement

Support of this work was provided by the National Science Foundation of the United States of America under Grant No. CMS-9253640 in association with a Presidential Faculty Fellow Award to D.A. Zumbunnen and in part by Award Number EEC-9731680.

### References

1. T. VIVIER and M. XANTHOS, *J. Appl. Polym. Sci.* **54** (1994) 596.
2. M. A. RAMOS and E. P. COLLAR, *J. Polym. Eng.* **7** (1987) 137.
3. M. C. SCHWARZ, J. W. BARLOW and D. R. PAUL, *J. Appl. Polym. Sci.* **35** (1988) 2053.
4. J. W. TEH and A. RUDIN, *Polym. Eng. Sci.* **31** (1991) 1033.
5. J. T. LINDT, A. K. GHOSH, *ibid.* **32** (1992) 1802.
6. A. P. PLOCHOCKI, S. S. DAGLI and R. D. ANDREWS, *ibid.* **30** (1990) 741.
7. C. E. SCOTT and C. W. MACOSKO, *Polymer Bulletin* **26** (1991) 341.
8. U. SUNDARARAJ, C. W. MACOSKO, R. J. ROLANDO and H. T. CHAN, *Polym. Eng. Sci.* **32** (1992) 1814.
9. N. CHAPLEAU and B. D. FAVIS, *J. Mater. Sci.* **30** (1995) 142.
10. H. A. STONE, B. J. BENTLEY and L. G. LEAL, *J. Fluid Mech.* **173** (1986) 131.
11. M. TIAHJADI and J. M. OTTINO, *ibid.* **232** (1991) 191.
12. K. C. MILES, B. NAGARAJAN and D. A. ZUMBRUNNEN, *J. Fluids Eng.* **117** (1995) 582.
13. D. A. ZUMBRUNNEN, K. C. MILES and Y. H. LIU, *Composites Part A* **27A** (1996) 37.
14. Y. H. LIU and D. A. ZUMBRUNNEN, *Polymer Composites* **17** (1996) 187.
15. D. F. ZHANG and D. A. ZUMBRUNNEN, *J. Fluids Eng.* **118** (1996) 40.
16. D. F. ZHANG, Y. H. LIU and D. A. ZUMBRUNNEN, *AIChE J.* **44** (1998) 442.
17. F. H. LING, *Physics Letters* **177A** (1993) 331.
18. M. LIU, F. J. MUZZIO and R. L. PESKIN, *Chaos, Solitons & Fractals* **4** (1994) 869.
19. C. W. LEONG, PhD dissertation, University of Massachusetts, 1990.
20. T. APPLEBY *et al.* *Polymer Bulletin* **32** (1994) 479.
21. M. WELANDER and M. RIGDAHL, *Polymer* **30** (1989) 207.
22. C. R. LINDSEY, D. R. PAUL and J. W. BARLOW, *J. Appl. Polym. Sci.* **26** (1981) 1.
23. H. A. STONE and L. G. LEAL, *J. Fluid Mech.* **198** (1989) 399.

Received 27 January 1997  
and accepted 6 October 1998